Electronic supplementary materials *Mendeleev Commun.*, 2022, **32**, 360–363

Positive and negative AMPA receptor modulators based on tricyclic bispidine derivative: minor structural change inverts the type of activity

Mstislav I. Lavrov, Polina N. Veremeeva, Elena A. Golubeva, Eugene V. Radchenko, Vladimir L. Zamoyski, Vladimir V. Grigoriev and Vladimir A. Palyulin

Table of contents

1. Chemistry

NMR spectra were recorded on the Agilent 400-MR spectrometer (400.0 MHz for ^{1}H; 100.6 MHz for ^{13}C) at room temperature; chemical shifts (δ) were measured with reference to the solvent $CDCl_3$ for ^{1}H (δ = 7.26 ppm), ^{13}C (δ = 77.16 ppm). Chemical shifts (δ) are given in ppm; J values are given in Hz. When necessary, assignments of signals in NMR spectra were made using 2D techniques. Accurate mass measurements (HRMS) were performed on a Bruker micrOTOF II instrument using electrospray ionization (ESI). The measurements were done in a positive ion mode (interface capillary voltage 4500 V) or in a negative ion mode (3200 V). Analytical thin layer chromatography was carried out with Silufol silica gel plates (supported on aluminum); the detection was done by UV lamp (254 and 365 nm) and chemical staining (5% aqueous solution of $KMnO_4$). Column chromatography was performed on silica gel (230–400 mesh, Merck).

Bispidine derivatives **2a** and **2b** were synthesized by previously described methods.[S1] All other starting materials were commercially available.

1,3-Benzodioxole-5-carbonyl chloride. A mixture of 1,3-benzodioxole-5-carboxylic acid (33.1 g, 0.195 mol) and thionyl chloride (85 ml, 1.170 mol, 6-fold excess) with the addition of pyridine (0.500 ml) was stirred under heating at 50 °C for 15 h. The solution was cooled to room temperature and the excess of thionyl chloride was distilled off. This yielded 36.0 g (0.195 mol, 98%) of pure 1,3-benzodioxole-5-carbonyl chloride as a white crystalline product. ^{1}H NMR (400 MHz, $CDCl_3$), δ: 6.11 (s, 2H), 6.89 (d, 1H, J 8.38 Hz), 7.49 (d, 1H, J 1.89 Hz), 7.78 (dd, 1H, J 8.31 Hz, J 1.96 Hz).

1,3-Benzodioxole-5-carboxamide. To a solution of 1,3-benzodioxole-5-carbonyl chloride (5.0 g, 0.027 mol) in dioxane (25 ml), a concentrated solution of aqueous ammonia (34 ml, 0.453 mol) was added dropwise with stirring. The reaction mixture was poured into distilled water (30 ml) while cooling with ice, and 12% HCl solution was added to pH 6. The precipitate formed was filtered off and washed with distilled water. The product was recrystallized from EtOH (30 ml). This yielded 2.5 g (0.015 mol, 56%) of pure 1,3-benzodioxole-5-carboxylic acid amide as colorless crystals. ^{1}H NMR (400 MHz, $CDCl_3$), δ: 5.80 (br. s, 2H), 6.05 (s, 2H), 6.85 (d, 1H, J 8.07 Hz), 7.32 (s, 1H), 7.36 (dd, 1H, J 8.07 Hz, J 1.56 Hz).

1,3-Benzodioxol-5-amine **1**. To a solution of NaOH (3.2 g, 80.0 mmol) in distilled water (24 ml), bromine (0.75 ml, 14.6 mmol) was added with stirring and ice-cooling. To the resulting solution, 1,3-benzodioxole-5-carboxamide (1.1 g, 6.7 mmol) was added portionwise, and the mixture was stirred for 2 h with cooling. The mixture was then heated to 60 °C and stirred for 15 min. The precipitate formed was filtered off, the filtrate was extracted with $CHCl_3$, and the solvent was distilled off. The resulting product was purified by column chromatography (eluent $CHCl_3$). This yielded 166 mg (1.2 mmol, 32%) of **1**. ^{1}H NMR (400 MHz, $CDCl_3$), δ: 3.29 (br. s, 2H), 5.86 (s, 2H), 6.13 (dd, 1H, J 8.16 Hz, J 2.29 Hz), 6.29 (d, 1H, J 2.32 Hz), 6.62 (d, 1H, J 8.19 Hz).

6-(1,3-Benzodioxol-5-yl)-1,11-dimethyl-3,6,9-triazatricyclo[7.3.1.1^{3,11}]tetradecane-4,8,12-trione **3a**. To a solution of compound **2a** (395 mg, 1.23 mmol) and 1,3-benzodioxol-5-amine **1** (166 mg, 1.21 mmol) in DMF (5.5 ml), K_2CO_3 (665 mg, 4.8 mmol) was added, and the mixture was stirred at 70 °C for 17 h. Then the reaction mixture was filtered, and the solvent was distilled off. The resulting product was purified by column chromatography (eluents $CHCl_3$ and $CHCl_3$/EtOH (50:1)). This yielded 64 mg (0.17 mmol, 18%) of **3a**. ^{1}H NMR (400 MHz, $CDCl_3$), δ: 1.06 (d, 6H), 2.84 (d, 2H, J 13.45 Hz), 3.22 (d, 2H, J 13.45 Hz), 3.85 (d, 2H, J 14.73 Hz), 4.20 (d, 2H, J 14.67 Hz), 4.99 (m, 4H), 5.99 (s, 2H), 6.56 (dd, 1H, J 8.31 Hz, J 2.32 Hz), 6.69 (d, 1H, J 2.32 Hz), 6.80 (d, 1H, J 8.31 Hz). ^{13}C NMR (100.6 MHz, $CDCl_3$), δ: 15.70, 15.81, 44.98, 45.66, 54.07, 55.35, 60.24, 101.04, 101.16, 108.37, 111.61, 143.82, 144.50, 148.42, 167.28, 210.28. HRMS (ESI), m/z 386.1710 (calc. for $C_{20}H_{23}N_3O_5$ [*M*+H]$^+$, m/z: 386.1710).

6-(1,3-Benzodioxol-5-yl)-1,11-dimethyl-3,6,9-triazatricyclo[7.3.1.1^{3,11}]tetradecane-4,8-dione **3b**. To a solution of compound **2b** (750 mg, 2.44 mmol) and 1,3-benzodioxol-5-amine **1** (267 mg, 1.95 mmol) in DMF (10 ml), K_2CO_3 (1.083 g, 7.84 mmol) was added, and the mixture was stirred at 75 °C for 20 h. Then the reaction mixture was diluted with distilled water (250 ml), extracted with $CHCl_3$, and the solvent was distilled off. The resulting product was purified by column chromatography (eluents $CHCl_3$ and $CHCl_3$/EtOH (50:1)). Thereafter, the product was further purified by recrystallization from ethyl acetate with precipitation with *n*-hexane. This yielded 62 mg (0.17 mmol, 12%) of pure **3b** as white crystals. ^{1}H NMR (400 MHz, $CDCl_3$), δ: 0.88 (d, 6H), 1.48 (s, 2H), 2.48 (d, 2H, J 12.96 Hz), 2.86 (d, 2H, J 12.90 Hz), 3.72 (d, 2H, J 14.24 Hz), 4.11 (d, 2H, J 14.00 Hz), 4.50 (d, 2H, J 12.78 Hz), 4.62 (d, 2H, J 12.96 Hz), 5.95 (s, 2H), 6.52 (d, 1H, J 7.95 Hz), 6.67 (s, 1H), 6.76 (d, 1H, J 8.25 Hz). ^{13}C NMR (100.6 MHz, $CDCl_3$), δ: 23.45, 23.83, 28.86, 29.30, 48.52, 52.35, 54.33, 60.20, 100.91, 101.02, 108.24, 111.28, 143.26, 144.89, 148.23, 167.03. HRMS (ESI), m/z 372.1911 (calc. for $C_{20}H_{25}N_3O_4$ [*M*+H]$^+$, m/z: 372.1918).

2. NMR Spectra

^{1}H NMR: 1,3-benzodioxole-5-carbonyl chloride

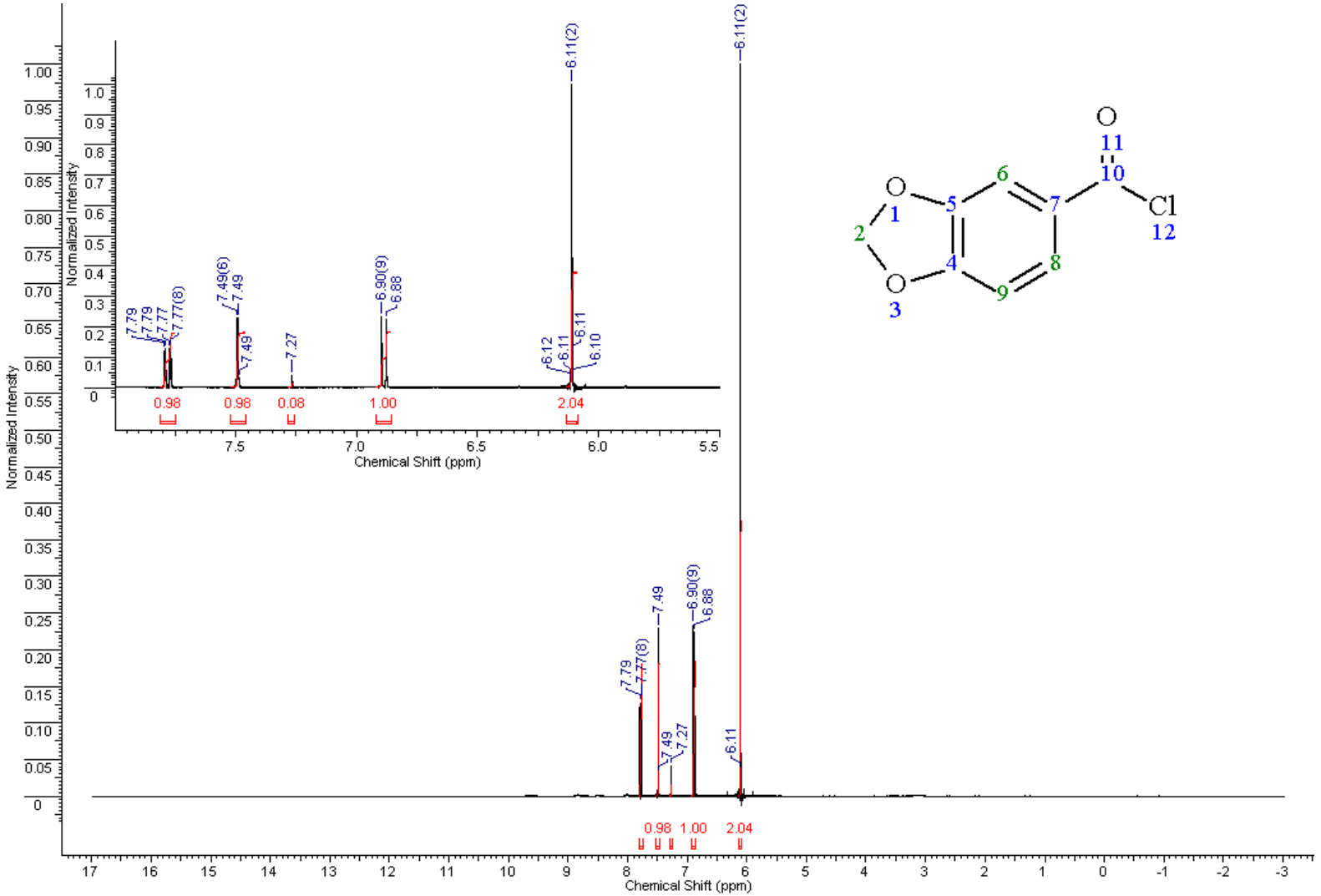

^{1}H NMR: 1,3-benzodioxole-5-carboxylic acid amide

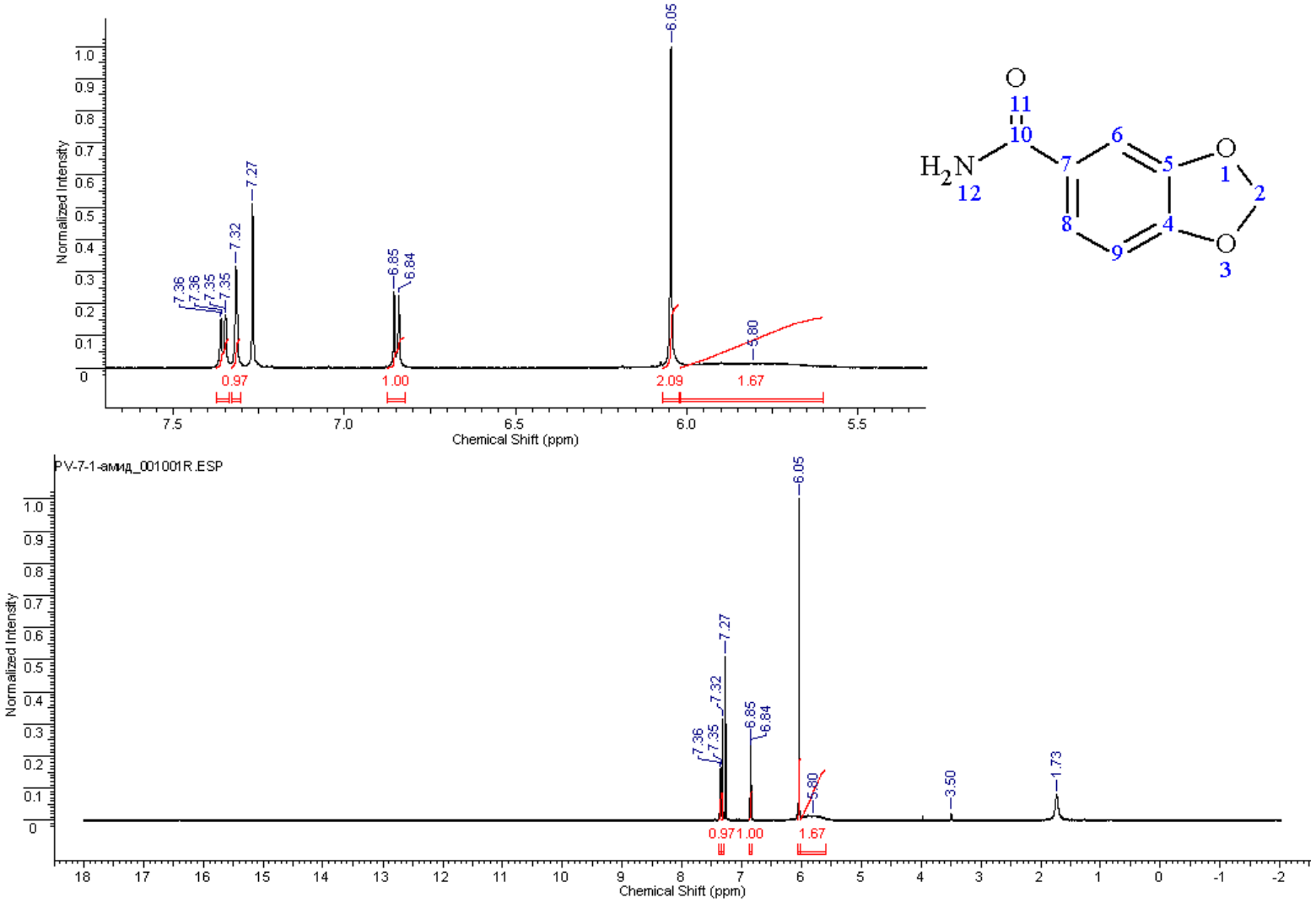

^{1}H NMR: compound **1**

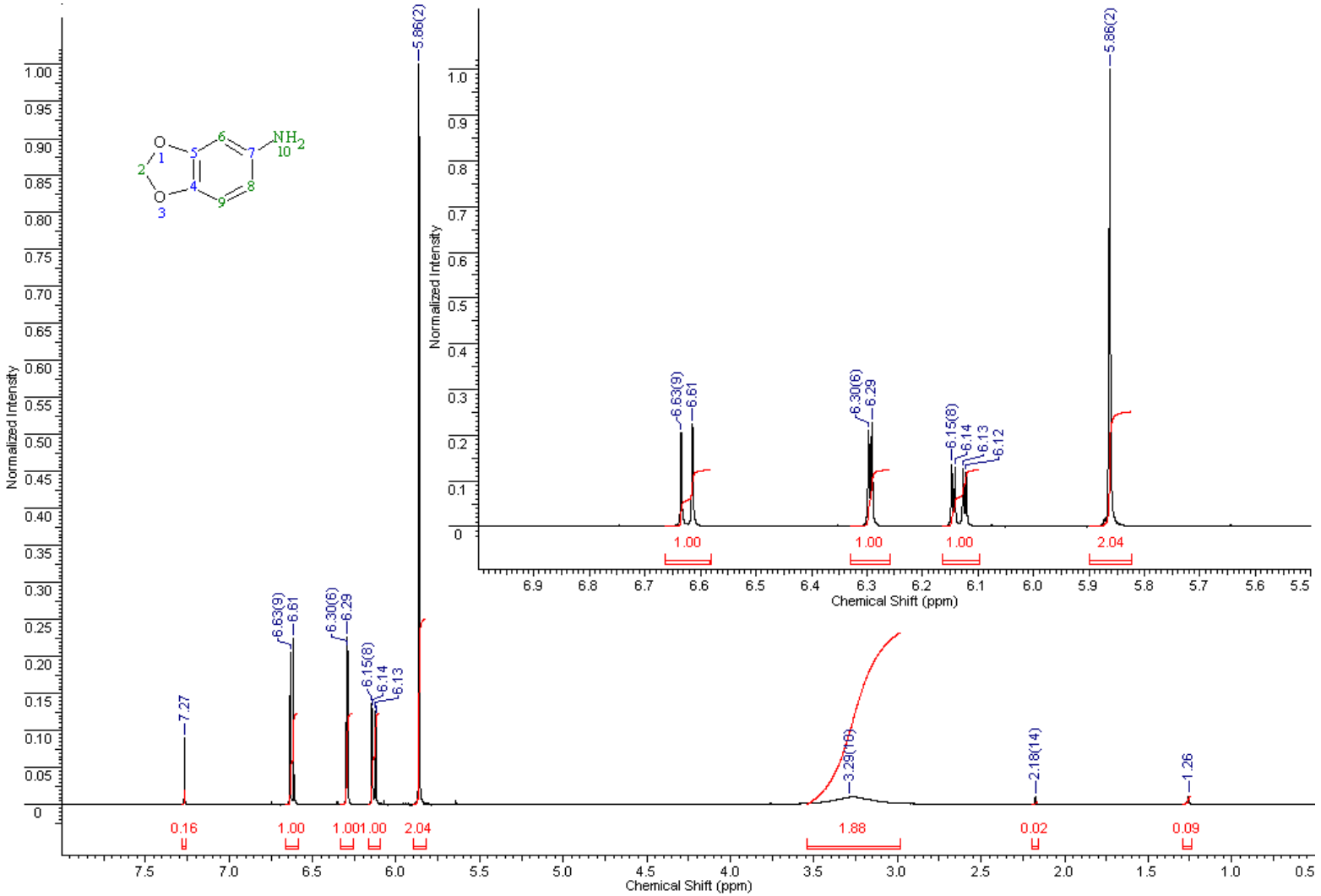

^{1}H NMR: compound **3a**

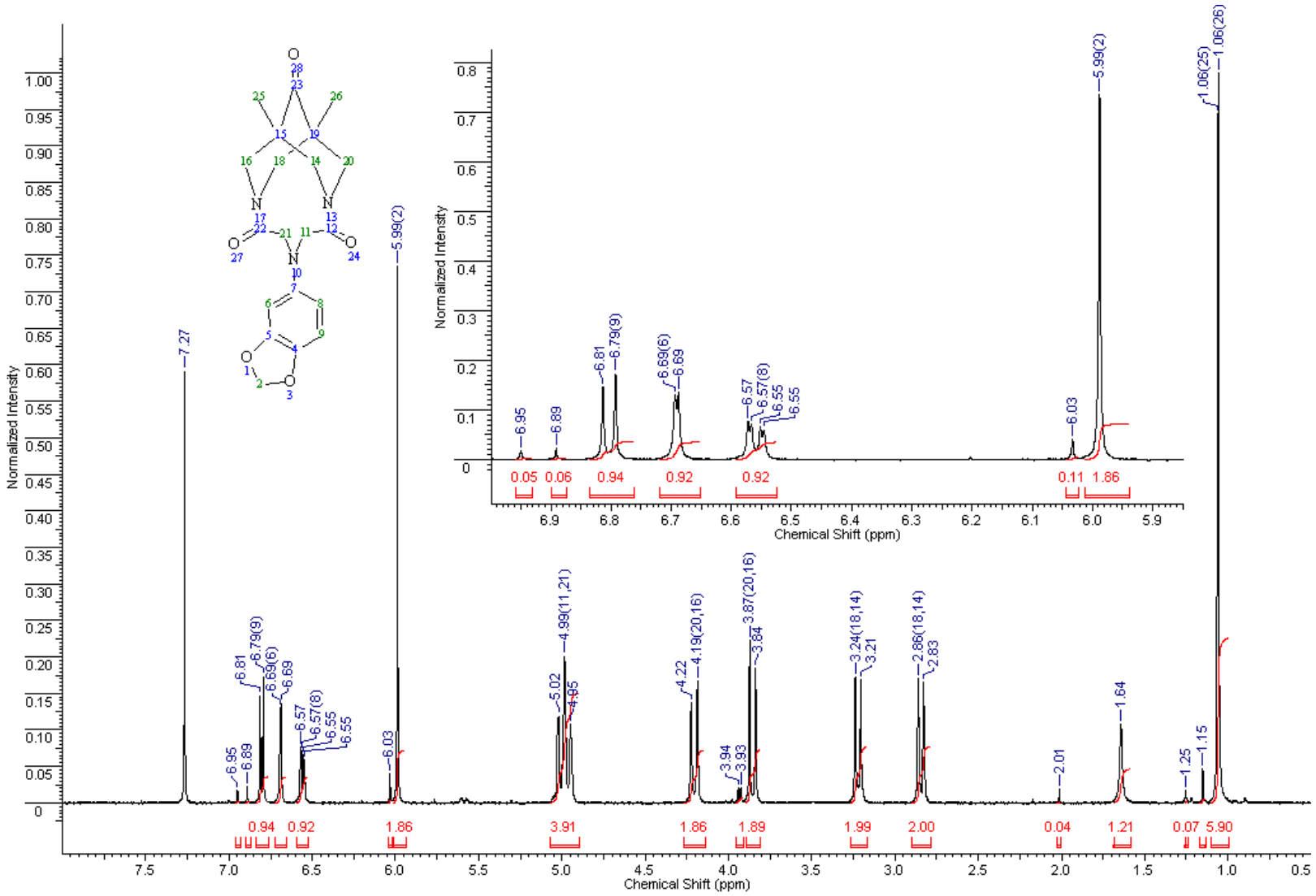

^{1}H NMR: compound **3b**

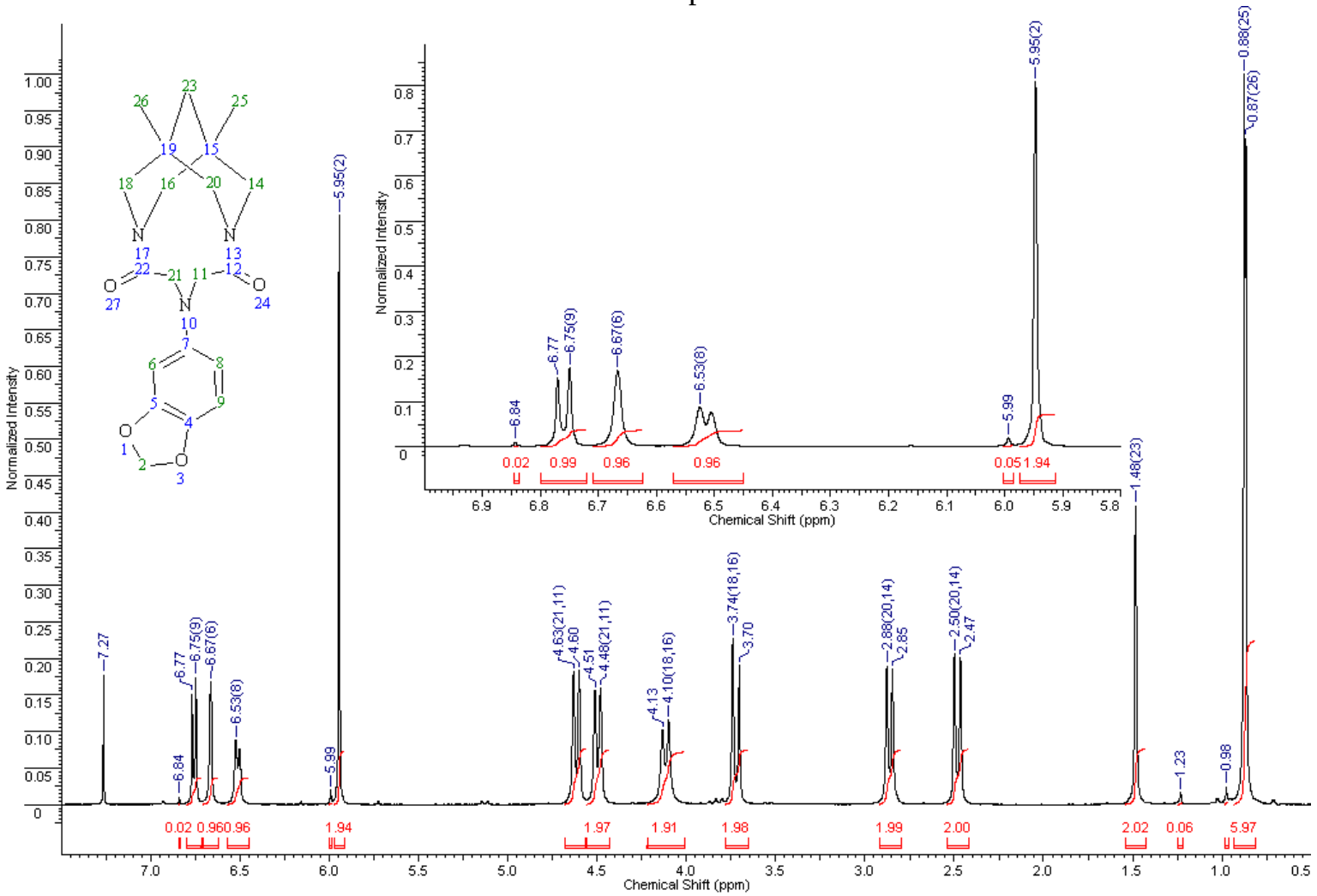

^{13}C NMR: compound **3a**

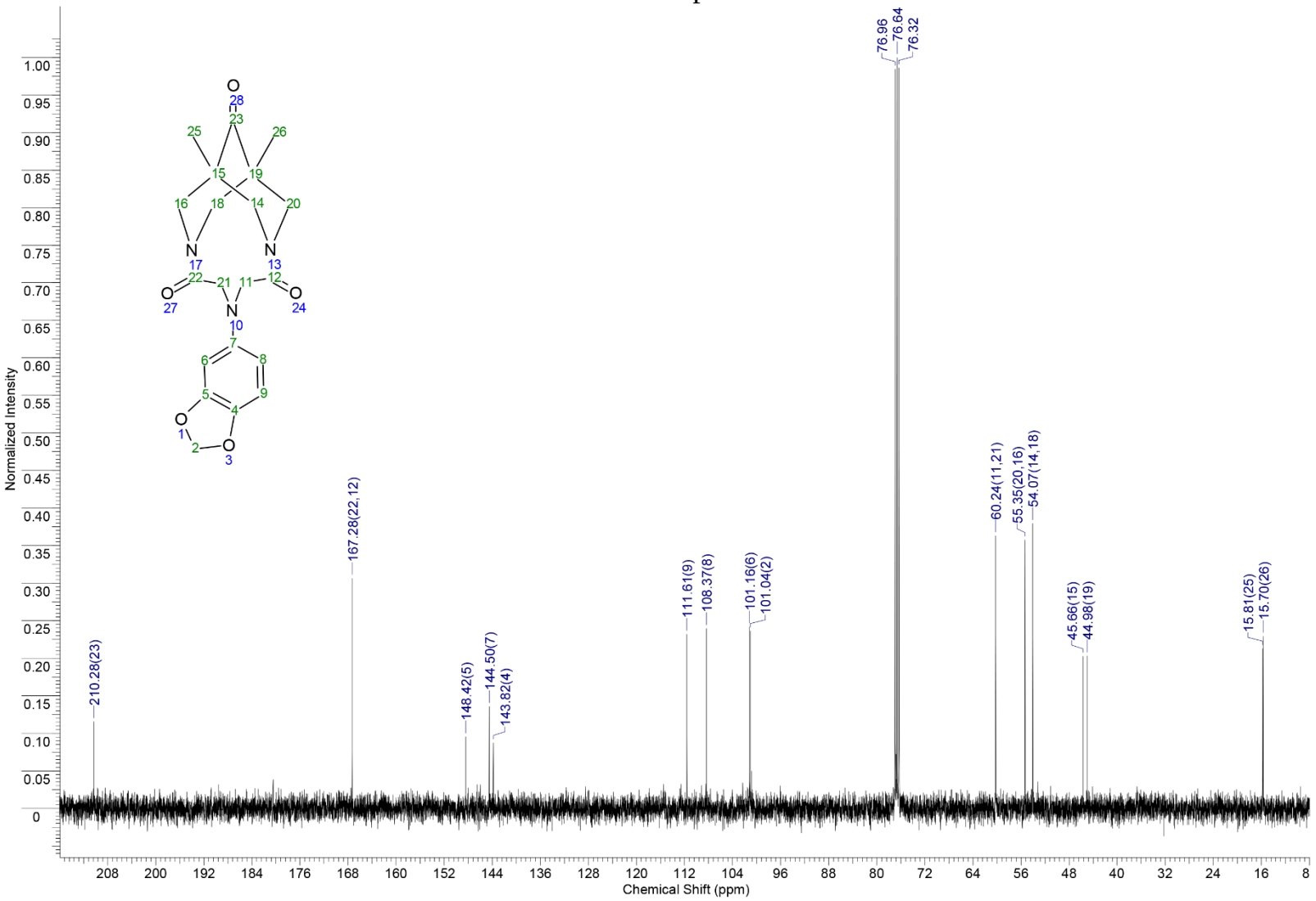

^{13}C NMR: compound **3b**

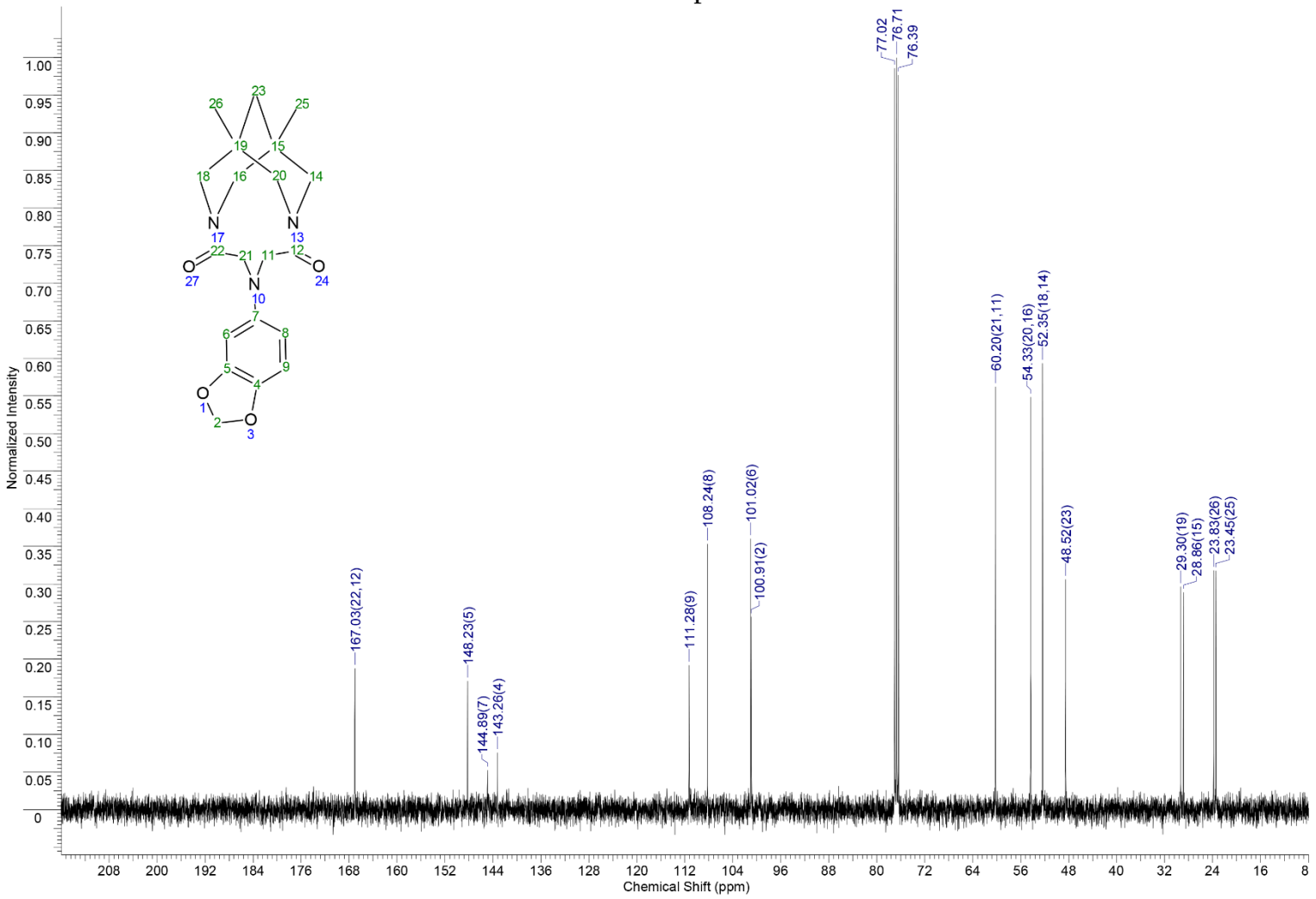

3. Electrophysiological studies

In vitro electrophysiological experiments were carried out using a patch clamp technique with local fixation of potential as described earlier.[S2,S3] Freshly isolated single Purkinje neurons from the cerebellum of 12–15 day old Wistar rats were used as a test system. Transmembrane currents were induced by the activation of AMPA receptors with a solution of their partial agonist kainic acid using fast superfusion of solutions, where 30 μL of the agonist buffer (the agonist concentration was varied in the range of 10^{-6}–10^{-4} M) were added to the constant flow of neuron-washing buffer. The applications for control and each compound concentration were done in triplicate. The transmembrane currents for individual neurons were recorded using 2.5–5.5 MΩ borosilicate microelectrodes in a whole-cell configuration with an EPC-9 device from HEKA, Germany. The data were processed by a Pulsfit program from HEKA, Germany.

The study was conducted according to the guidelines of the Declaration of Helsinki and approved by the Institutional Animal Review Board of IPAC RAS.

4. Molecular modelling

PAM binding site

The structure of the dimeric ligand-binding domain of the rat GluA2 AMPA receptor was obtained from the Protein Data Bank (PDB: 4FAT).[S4] Upon removal of ions and small molecules (except the two bound glutamate agonist molecules), the protein was allowed to relax during molecular dynamics simulation for 100 ns (see below for the simulation protocol). The most frequently occurring structure was identified by clustering of the frames in the stable part of the trajectory (40–100 ns). The ligand structures were converted to 3D and preoptimized in the MMFF94 force field using Avogadro 1.2.0 software,[S5] and then the ligand and protein structures were prepared for molecular docking using AutoDock Tools 1.5.6 software.[S6] Molecular docking into the positive allosteric modulator binding site was performed with AutoDock Vina 1.1.2 software[S7] (grid box size 22 Å × 29 Å × 40 Å, exhaustiveness = 16). The pose with the best scoring function value and ligand position was selected and the complex model was built using the UCSF Chimera 1.15 software.[S8]

The molecular dynamics simulations were performed using the CHARMM36 / CGenFF 4.4 force field[S9,S10] in the GROMACS 2021.2 software.[S11] The initial models of the systems were built using the Ligand Reader & Modeler and Solution Builder modules of the CHARMM-GUI web service.[S12,S13] The protein molecule was inserted into a rectangular periodic boundary box of water in the TIP3P model; the distance from the protein to the box border was no less than 10 Å. Individual randomly selected water molecules were replaced with potassium and chlorine ions to ensure electrical neutrality of the system and the total concentration of KCl about 0.15 M. For each system, the molecular mechanics minimization (up to 5000 steps) was performed on the CPU, followed by equilibration for 125 ps with integration timestep of 1 fs at the temperature of 300 K and constant volume using the v-rescale thermostat on the NVIDIA GeForce RTX 3080 GPU. The production simulation was performed on the GPU with integration timestep of 2 fs at the temperature of 300 K and the constant pressure of 1 atm using the v-rescale thermostat and the Parrinello–Rahman barostat. The hydrogen atom movements were constrained using the LINCS algorithm. For the analysis and visualization of the results, the cpptraj software[S14] in the AmberTools 21 package[S15] and UCSF Chimera were used.

The plots of the root mean square deviations (RMSD) for the protein, glutamate, and ligand heavy atoms (Figure S1) as well as the visual inspection of the trajectories confirm that the system stability is retained over the entire course of the production simulation (200 ns). The position of the ligand **3a** in the PAM binding site at the interface between the dimeric ligand-binding domains is slightly adjusted compared to the docking pose, and its binding mode remains stable over the entire course of the simulation. Similar to other medium-sized modulators,[S16] the **3a** molecule occupies a symmetrical position in the central subpocket of the symmetrical PAM binding site (main text

Figure 2, *a*, *b*). The binding is primarily stabilized by hydrophobic interactions and steric fit with additional contribution from the electrostatic interaction between the ligand's carbonyl group and the positively charged Lys616 residue (Figure 2, *b*, *c*). On the other hand, the binding stability of the compound **3b** is much lower, it undergoes partial dissociation and eventually attains a loosely anchored position in the cleft between the ligand-binding domains (Figure 2, *d*, *e*, *f*).

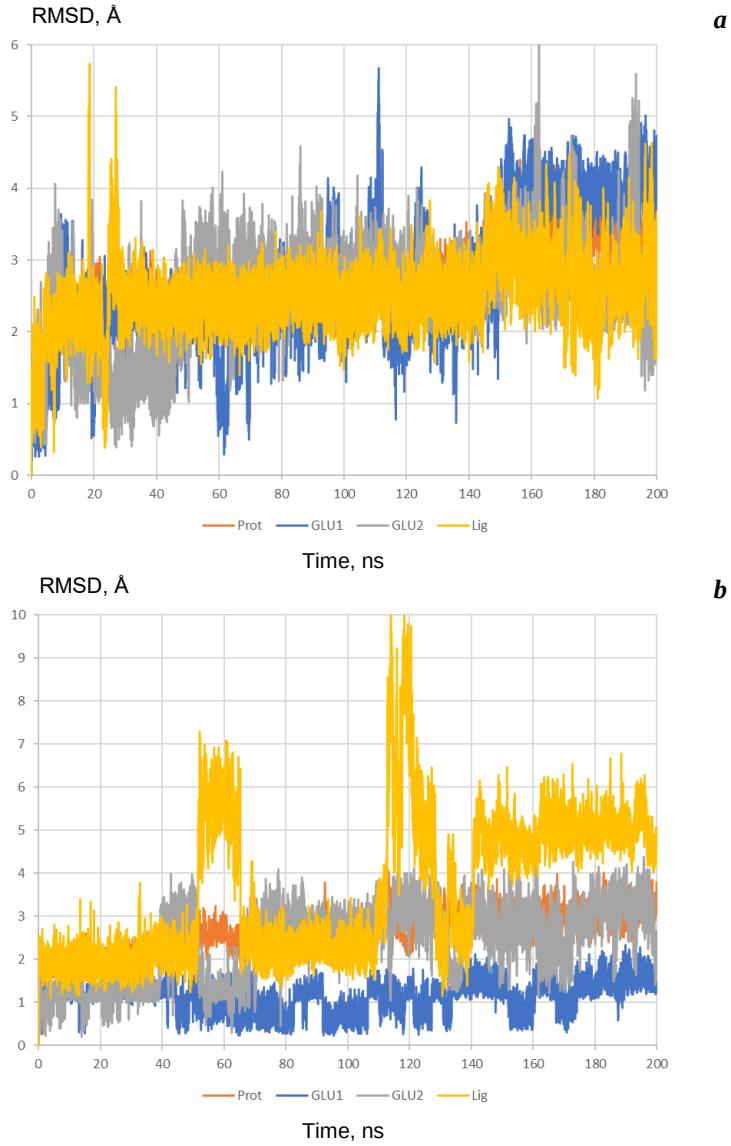

Figure S1 RMSD of the protein, glutamate, and ligand **3a** (*a*) and **3b** (*b*) heavy atoms during molecular dynamics simulation of their complexes with the PAM binding site of the dimeric ligand-binding domain of the GluA2 AMPA receptor.

The binding free energies were estimated over the stable portion of the trajectories (last 20 ns, 101 frames at 200 ps interval) using the MM/GBSA approach implemented in the gmx_MMPBSA 1.4.3 software.[S17,S18] The internal dielectric constant $\varepsilon = 4$ and the Interaction Entropy model for the conformation entropy contribution were used. The resulting energy values are listed in Table S1.

Overall, these results indicate that the compound **3a** can indeed act as a positive AMPA receptor modulator binding in the validated PAM binding site while the compound **3b** can be expected to have much weaker PAM activity.

Table S1 Binding free energy for compounds **3a** and **3b** calculated using MM/GBSA approach.

Energy terms, kcal mol^{-1}	Compound **3a**	Compound **3b**
ΔE_{int}	0±0	0±0
ΔE_{ele}	–1.6±0.2	–5.5±0.1
ΔE_{vdw}	–33.5±0.3	–28.8±0.2
$\Delta E_{MM} = \Delta E_{int} + \Delta E_{ele} + \Delta E_{vdw}$	–35.1±0.3	–34.4±0.2
ΔG_{GB}	6.8±0.1	10.4±0.1
ΔG_{SA}	–4.23±0.03	–3.64±0.03
$\Delta G_{sol} = \Delta G_{GB} + \Delta G_{SA}$	2.6±0.1	6.8±0.1
$\Delta G_{MMGBSA} = \Delta E_{MM} + \Delta G_{sol}$	–32.5±0.3	–27.6±0.2
$- T\Delta S$	4.2±0.1	3.6±0.1
$\Delta G_b = \Delta G_{MMGBSA} - T\Delta S$	–28.4±0.3	–24.0±0.2

Note: Values are listed as Mean ± Standard Error of Mean.

NAM binding site

The structure of the tetrameric rat GluA2 AMPA receptor complexed with four Perampanel molecules at the interface between the ligand-binding (LBD) and transmembrane (TMD) domains was obtained from the Protein Data Bank (PDB: 5L1F).[S19] To enable meaningful and efficient molecular dynamics simulations, a tetrameric LBD-TMD fragment was modelled from this structure and the canonical protein sequence (UniProt: P19491) using the Modeller 10.1 software.[S20] The modifications of the receptor structure included removal of small molecules, removal of the extracellular N-terminal domains and cytoplasmic C-terminal tails, reconstruction of the missing and unresolved residues, and reduction of the cytoplasmic M1–M2 loop (see sequence alignment in Figure S2).

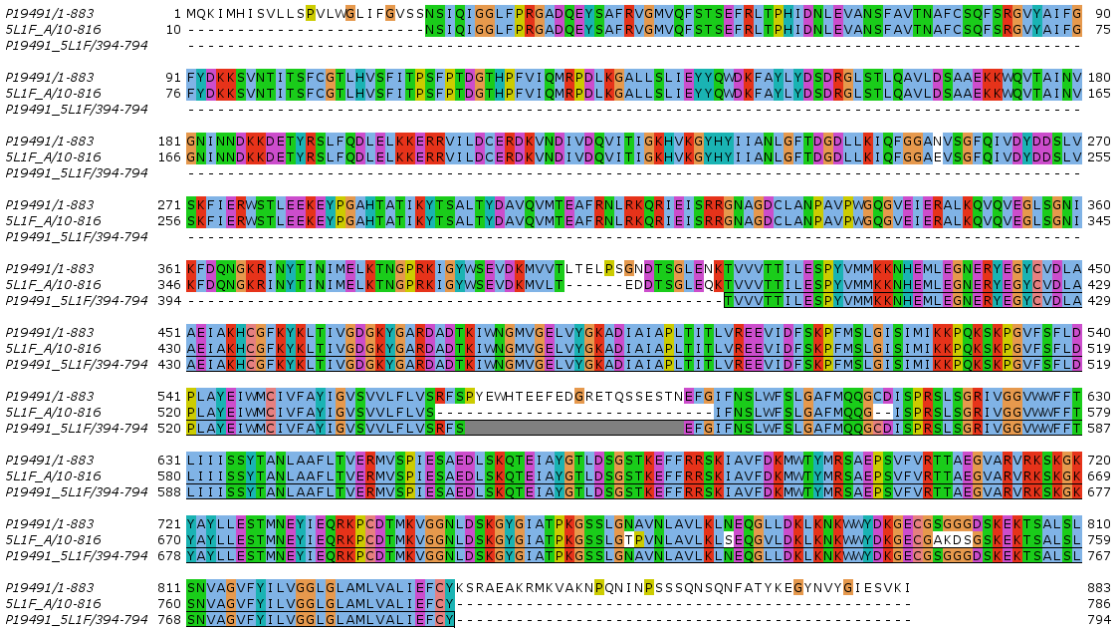

Figure S2 Aligned protein sequences of the rat GluA2 AMPA receptor (P19491, canonical sequence; 5L1F_A, representative sequence of the template PDB structure; P19491_5L1F, LBD-TMD fragment used in the modelling). The ClustalX coloring scheme is used; the removed section of the cytoplasmic M1–M2 loop is shown in grey.

The ligand structures were converted to 3D and preoptimized in the MMFF94 force field using Avogadro 1.2.0 software,[S5] and then the ligand and protein structures were prepared for

molecular docking using AutoDock Tools 1.5.6 software.[S6] Molecular docking into the negative allosteric modulator binding sites (four symmetrical sites) was performed with AutoDock Vina 1.1.2 software[S7] (grid box size 18 Å × 18 Å × 18 Å, exhaustiveness = 16). The poses with the best scoring function value and ligand position were selected and the complex model was built using the UCSF Chimera 1.15 software.[S8]

The molecular dynamics simulations were performed using the CHARMM36 / CGenFF 4.4 force field[S9,S10] in the GROMACS 2021.2 software.[S11] The initial models of the systems were built using the Ligand Reader & Modeler and Bilayer Builder modules of the CHARMM-GUI web service.[S12,S13] The protein was embedded into the rectangular 1-palmitoyl-2-oleoyl-*sn*-glycero-3-phosphocholine (POPC) lipid bilayer (approximate size 120 Å × 120 Å) and inserted into a rectangular periodic boundary box of water in the TIP3P model; the distance from the protein to the top and bottom box border was no less than 22.5 Å. Individual randomly selected water molecules were replaced with potassium and chlorine ions to ensure electrical neutrality of the system and the total concentration of KCl about 0.15 M. For each system, the molecular mechanics minimization (up to 5000 steps) was performed on the CPU, followed by equilibration at the temperature of 300 K on the NVIDIA GeForce RTX 3080 GPU. In total, 6 equilibration steps were performed with sequential relaxing of the forces restraining the movements of the protein, ligand, and lipid atoms. (The first 2 steps of 125 ps each were done at constant volume using the Berendsen thermostat, followed by 1 step of 125 ps and 3 steps of 500 ps each at constant pressure of 1 atm using the Berendsen thermostat and the Berendsen barostat; the integration timestep was 1 fs for equilibration steps 1–3 and 2 fs for equilibration steps 4–6). The production simulation was performed on the GPU with integration timestep of 2 fs at the temperature of 300 K and the constant pressure of 1 atm using the v-rescale thermostat and the Parrinello–Rahman barostat. The hydrogen atom movements were constrained using the LINCS algorithm. For the analysis and visualization of the results, the cpptraj software[S14] in the AmberTools 21 package[S15] and UCSF Chimera were used.

The plots of the root mean square deviations (RMSD) for the protein and ligand heavy atoms (Figure S3) as well as the visual inspection of the trajectories confirm that overall stability of the system is retained over the entire course of the production simulation (200 ns). However, one of the LBD dimers is significantly deflected (possibly due to the lack of stabilization from the N-terminal domains) and, in the ligand **3b** complex, the arrangement of the transmembrane domains is somewhat disrupted. Some of the modulator molecules are stably bound while others can undergo significant displacement from their docking poses or leave the binding site (Figure S4). At this time, no significant differences in the behavior of the compounds can be conclusively detected. Nevertheless, these results can suggest that the NAM activity of compound **3b** can be mediated by its action on the NAM binding sites at the LBD-TMD interface that might be less pronounced in the case of compound **3a**.

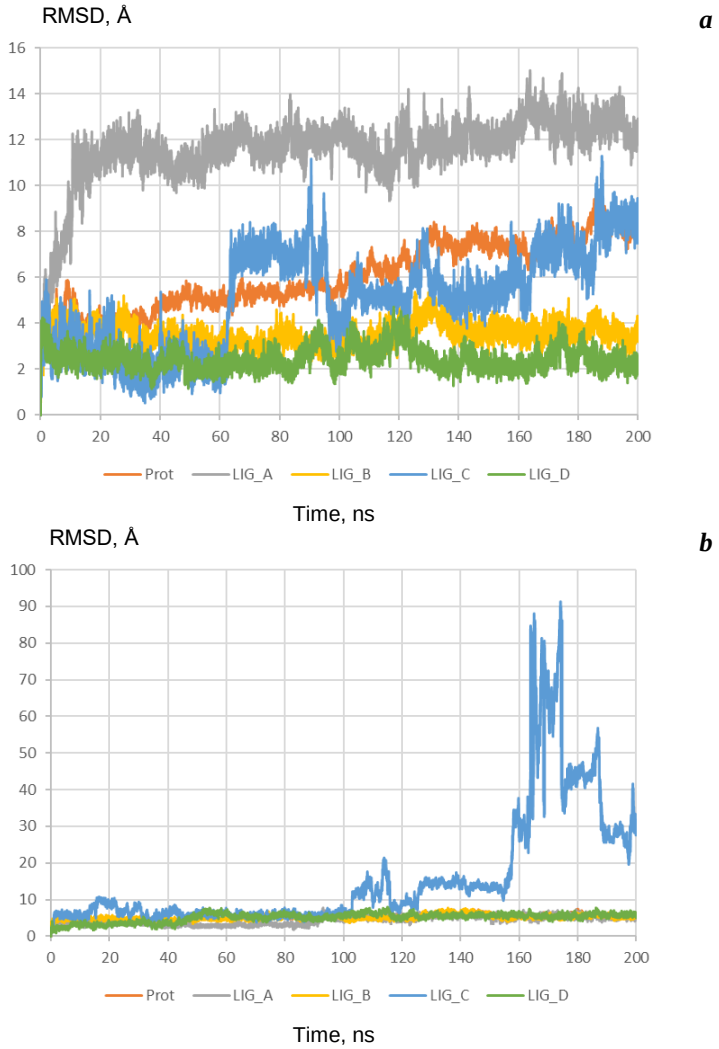

Figure S3 RMSD of the protein and ligand **3a** (*a*) and **3b** (*b*) heavy atoms during molecular dynamics simulation of their complexes with the NAM binding sites of the GluA2 AMPA receptor. The LIG_A–LIG_D notation refers to the ligand molecules bound to the corresponding receptor subunits.

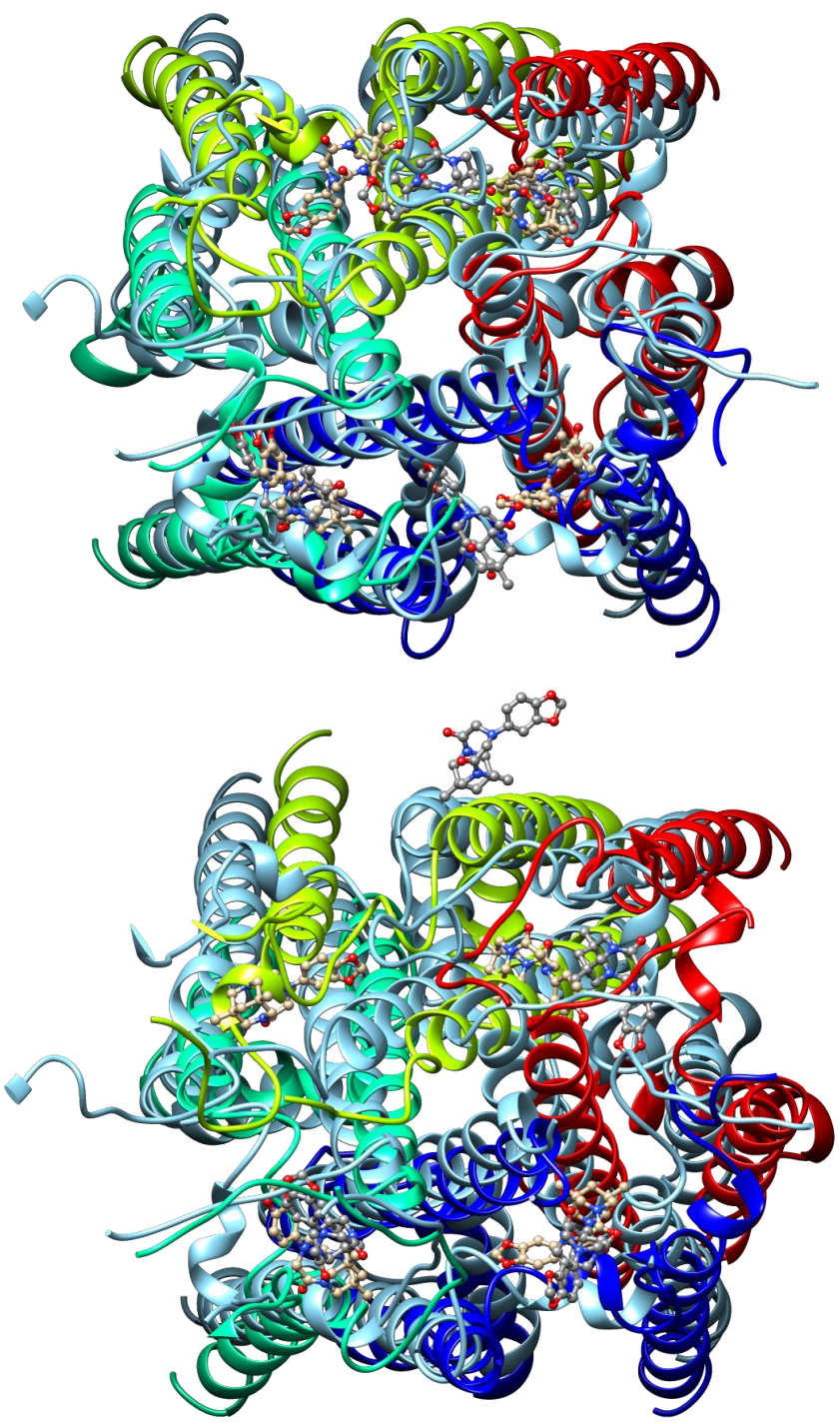

Figure S4 Comparison of the binding locations of ligands **3a** (*a*) and **3b** (*b*) in the NAM binding sites of the LBD-TMD fragment of GluA2 AMPA receptor (for clarity, LBDs are not shown). The starting protein structure and docked ligand poses are shown as light blue ribbons and beige ball-and-stick models. The structure and ligand positions obtained after molecular dynamics simulations are shown as subunit-colored ribbons (blue, mint, green, red) and dark grey ball-and-stick models.

References

S1 P. N. Veremeeva, I. V. Grishina, O. V. Zaborova, A. D. Averin and V. A. Palyulin, *Tetrahedron*, 2019, **75**, 4444.

S2 M. I. Lavrov, D. S. Karlov, T. A. Voronina, V. V. Grigoriev, A. A. Ustyugov, S. O. Bachurin and V. A. Palyulin, *Mol. Neurobiol.*, 2020, **57**, 191.

S3 N. S. Temnyakova, D. A. Vasilenko, M. I. Lavrov, D. S. Karlov, Y. K. Grishin, V. L. Zamoyski, V. V. Grigoriev, E. B. Averina and V. A. Palyulin, *Mendeleev Commun.*, 2021, **31**, 216.

S4 J. E. Harms, M. Benveniste, J. K. F. Maclean, K. M. Partin and C. Jamieson, *Neuropharmacology*, 2013, **64**, 45.

S5 M. D. Hanwell, D. E. Curtis, D. C. Lonie, T. Vandermeersch, E. Zurek and G. R. Hutchison, *J. Cheminform.*, 2012, **4**, 17.

S6 G. M. Morris, R. Huey, W. Lindstrom, M. F. Sanner, R. K. Belew, D. S. Goodsell and A. J. Olson, *J. Comput. Chem.*, 2009, **30**, 2785.

S7 O. Trott and A. J. Olson, *J. Comput. Chem.*, 2010, **31**, 455.

S8 E. F. Pettersen, T. D. Goddard, C. C. Huang, G. S. Couch, D. M. Greenblatt, E. C. Meng and T. E. Ferrin, *J. Comput. Chem.*, 2004, **25**, 1605.

S9 K. Vanommeslaeghe, E. Hatcher, C. Acharya, S. Kundu, S. Zhong, J. Shim, E. Darian, O. Guvench, P. Lopes, I. Vorobyov and A. D. Mackerell, *J. Comput. Chem.*, 2010, **31**, 671.

S10 J. Huang and A. D. MacKerell, *J. Comput. Chem.*, 2013, **34**, 2135.

S11 M. J. Abraham, T. Murtola, R. Schulz, S. Páll, J. C. Smith, B. Hess and E. Lindahl, *SoftwareX*, 2015, **1–2**, 19.

S12 S. Jo, T. Kim, V. G. Iyer and W. Im, *J. Comput. Chem.*, 2008, **29**, 1859.

S13 J. Lee, X. Cheng, J. M. Swails, M. S. Yeom, P. K. Eastman, J. A. Lemkul, S. Wei, J. Buckner, J. C. Jeong, Y. Qi, S. Jo, V. S. Pande, D. A. Case, C. L. Brooks, A. D. MacKerell, J. B. Klauda and W. Im, *J. Chem. Theory Comput.*, 2016, **12**, 405.

S14 D. R. Roe and T. E. Cheatham, *J. Chem. Theory Comput.*, 2013, **9**, 3084.

S15 R. Salomon-Ferrer, D. A. Case and R. C. Walker, *WIREs Comput. Mol. Sci.*, 2013, **3**, 198.

S16 T. Drapier, P. Geubelle, C. Bouckaert, L. Nielsen, S. Laulumaa, E. Goffin, S. Dilly, P. Francotte, J. Hanson, L. Pochet, J. S. Kastrup and B. Pirotte, *J. Med. Chem.*, 2018, **61**, 5279.

S17 M. S. Valdés-Tresanco, M. E. Valdés-Tresanco, P. A. Valiente and E. Moreno, *J. Chem. Theory Comput.*, 2021, **17**, 6281.

S18 B. R. Miller, T. D. McGee, J. M. Swails, N. Homeyer, H. Gohlke and A. E. Roitberg, *J. Chem. Theory Comput.*, 2012, **8**, 3314.

S19 M. V. Yelshanskaya, A. K. Singh, J. M. Sampson, C. Narangoda, M. Kurnikova and A. I. Sobolevsky, *Neuron*, 2016, **91**, 1305.

S20 A. Šali and T. L. Blundell, *J. Mol. Biol.*, 1993, **234**, 779.